

# Gelatin/bioactive glass composite scaffold for promoting the migration and odontogenic differentiation of bone marrow mesenchymal stem cells

Guibin Huang<sup>a</sup>, Liju Xu<sup>b,c</sup>, Jilin Wu<sup>a</sup>, Sainan Wang<sup>a,\*</sup>, Yanmei Dong<sup>a,\*\*</sup>

<sup>a</sup> Department of Cariology and Endodontology, Peking University School and Hospital of Stomatology & National Clinical Research Center for Oral Diseases & National Engineering Laboratory for Digital and Material Technology of Stomatology & Beijing Key Laboratory of Digital Stomatology, Beijing, 100081, PR China

<sup>b</sup> Beijing National Laboratory for Molecular Sciences, CAS Research/Education Center for Excellence in Molecular Sciences, Institute of Chemistry, Chinese Academy of Sciences, Beijing, 100190, PR China

<sup>c</sup> University of Chinese Academy of Sciences, Beijing, 100190, PR China

## ARTICLE INFO

### Keywords:

pH-neutral bioactive glass  
Composite scaffold  
Bone marrow mesenchymal stem cells  
Migration  
Odontogenic differentiation  
Pulp regeneration

## ABSTRACT

Recruiting periapical stem cells into the root canal and inducing their odontogenic differentiation are both vital for pulp regeneration. This study was aimed at developing a kind of bioactive composite scaffolds (G/PSC scaffolds) by combining the pH-neutral bioactive glass named PSC and gelatin. The incorporation of PSC endowed the scaffolds with bioactivity and enhanced its resistance to enzymatic hydrolysis *in vitro* while maintaining its high water absorption capacity. The G/PSC scaffold with a PSC content of 0.5 mg/mL in 3% gelatin solution showed the best overall performance, released large amounts of silicate ions and maintained a neutral pH after soaking in simulated body fluid (SBF). Human bone marrow mesenchymal stem cells (hBMMSCs) developed good cell morphology with affluent pseudopods on the G/PSC scaffold and infiltrated fairly deep into it. Additionally, hBMMSCs showed increased proliferation and mRNA expression levels of dentin sialophosphoprotein (DSPP), dentin matrix protein 1 (DMP-1), alkaline phosphatase (ALP), collagen type I (Col-1), osteocalcin (OCN), and runt-related transcription factor 2 (Runx2). The present results demonstrated that the G/PSC scaffold significantly promoted hBMMSC chemotaxis, proliferation and odontogenic differentiation. Therefore, the G/PSC scaffold is a promising material for pulp regeneration.

## 1. Introduction

Pulp regeneration is the ideal therapy for endodontic diseases but is hard to realize. A suitable source of mesenchymal stem cells (MSCs) is the most determining factor in pulp regeneration. Odontogenic stem cells involved in pulp regeneration mainly include dental pulp stem cells (DPSCs), stem cells from the apical papilla (SCAPs) and periodontal ligament stem cells (PDLSCs) [1]. However, endodontic diseases, including pulp necrosis and apical lesions, often lead to the destruction of pulp and periapical tissues, resulting in the loss of odontogenic stem cells. Thus, non-odontogenic stem cells such as bone marrow mesenchymal stem cells (BMMSCs) may play an important role in pulp regeneration. In pulp revascularization, BMMSCs from the jawbone can enter the root canal with the evoked blood after mechanical irritation of

periapical tissue [2,3]. The histologic results had revealed bone-like tissues in the root canal after pulp revascularization, suggesting that BMMSCs might participate in pulp regeneration [4]. MSCs are pluripotent stem cells, whose differentiation may be regulated by the micro-environment. Direct pulp capping in the mouse demonstrated that bone marrow-derived cells could differentiate into odontoblast-like cells in the pulp damage repair microenvironment and secrete reparative dentin matrix in the pulp healing process [5]. As reported previously, the combination of BMMSCs and embryonic oral epithelium or oral epithelial cells could stimulate an odontogenic response *in vitro* and form a tooth-like structure *in vivo* [6,7]. Tooth germ cell conditioned medium (TGC-CM) could induce odontogenic differentiation of BMMSCs via the ERK/MAPK signaling pathway [8]. Hence, BMMSCs have odontogenic potential under certain circumstances and may be a source of seed cells

\* Corresponding author. Department of Cariology and Endodontology, Peking University School and Hospital of Stomatology, 22 Zhongguancun South Avenue, Haidian District, Beijing, 100081, PR China.

\*\* Corresponding author. Department of Cariology and Endodontology, Peking University School and Hospital of Stomatology, 22 Zhongguancun South Avenue, Haidian District, Beijing, 100081, PR China.

E-mail addresses: [bdkqwsn@bjmu.edu.cn](mailto:bdkqwsn@bjmu.edu.cn) (S. Wang), [kqdongyanmei@bjmu.edu.cn](mailto:kqdongyanmei@bjmu.edu.cn) (Y. Dong).

<https://doi.org/10.1016/j.polymeresting.2020.106915>

Received 11 September 2020; Received in revised form 13 October 2020; Accepted 15 October 2020

Available online 20 October 2020

0142-9418/© 2020 The Author(s).

Published by Elsevier Ltd.

This is an open access article under the CC BY-NC-ND license

(<http://creativecommons.org/licenses/by-nc-nd/4.0/>).

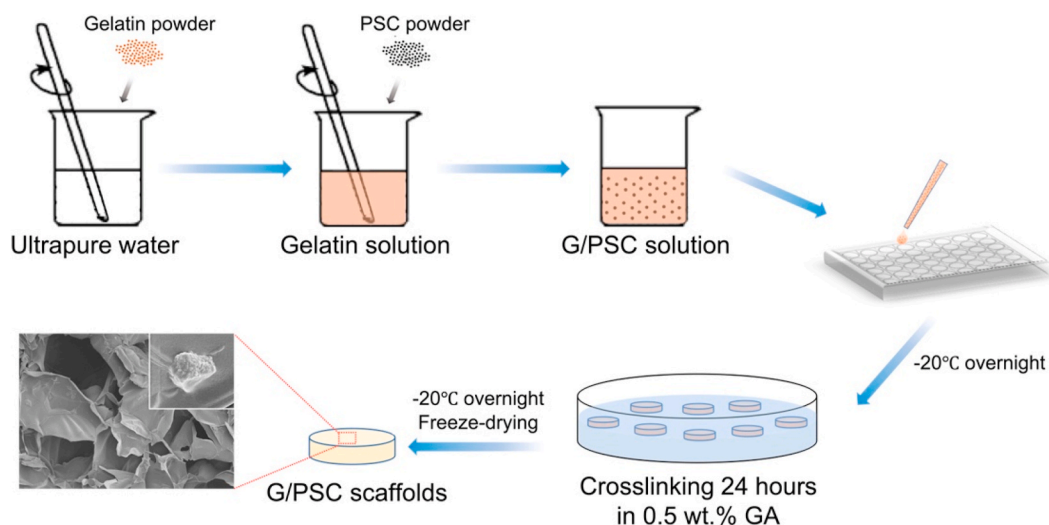


Fig. 1. The preparation of G and G/PSC scaffolds.

for pulp regeneration. However, newborn tissue is bone-like rather than dentin-like. A plausible reason might be the lack of appropriate odontogenic microenvironment. Therefore, creating a microenvironment suitable for the odontogenic differentiation of BMMSCs is essential.

Previous studies have reported that BMMSCs have the potential of odontogenic differentiation induced by signals from a suitable microenvironment, such as the embryonic oral epithelium, TGC-CM, natural dentin matrix and compressive scaffolds [6–10]. However, the chance of obtaining sufficient autologous embryonic oral epithelium, tooth germ cells or natural dentin matrix in the repairing site is extremely low. Additionally, allogeneic or xenogeneic implantation has more problems, including potential immunogenicity and ethical issues. The compressive scaffolds can initiate the odontogenic response in BMMSCs [10], suggesting that the microenvironment produced by artificial scaffolds could also provide induction signals for odontogenic differentiation. However, recruiting MSCs into the root canal is also extremely important for pulp regeneration besides inducing odontogenic differentiation. Therefore, biomaterials that can induce both BMMSC chemotaxis and odontogenic differentiation become the primary pursuit in pulp regeneration.

Gelatin is a natural origin protein with good biodegradability and biocompatibility but no immunogenicity [11]. Gelatin scaffolds were found to promote the adhesion and growth of human dental pulp cells (hDPCs). However, their high degradation rate and absence of odontogenic induction limited their application in pulp regeneration [12,13]. Our previous studies showed that bioactive glass (BG) not only had good mineralization and osteogenesis properties but also excellent odontogenesis and cell chemotaxis performances [14–17]. In particular, the pH-neutral bioactive glass named PSC was found to promote the proliferation, migration, odontogenic differentiation and mineralization of hDPCs and to induce the regeneration of the pulp-dentin complex-like structure from pulp tissue *in vivo* efficiently [18–20]. Therefore, the combination of PSC and gelatin may form a suitable material for pulp regeneration. In this study, we aimed to prepare gelatin/PSC composite scaffolds (G/PSC scaffolds) and evaluate their potential application for pulp regeneration *in vitro*.

## 2. Materials and methods

### 2.1. Materials

The pH-neutral bioactive glass which of named PSC were consisted of 10.8% P<sub>2</sub>O<sub>5</sub>–54.2% SiO<sub>2</sub>–35% CaO, mol%. The PSC particulates (Wooquick, Taizhou, China) were ground in an agate mortar, and a 1250-mesh sieve was used to obtain fine particles with a size  $\leq 10 \mu\text{m}$

(Fig. S1). Gelatin (from porcine skin; Type A;  $\sim 300$  g Bloom) was purchased from Sigma-Aldrich (Sigma-Aldrich, USA). Water (18.2 M $\Omega$ ) was obtained using an ultrapure water system (Millipore, USA). Mesenchymal Stem Cell Medium (MSCM), fetal bovine serum (FBS), Penicillin-Streptomycin solution and Mesenchymal Stem Cell Growth Supplement (MSCGS) were purchased from ScienCell Research Laboratories (San Diego CA, USA). Trypsin-EDTA (0.25%) and phosphate-buffered saline (PBS) were acquired from Gibco (Grand Island, USA).

### 2.2. Preparation of scaffolds

The G/PSC composite scaffolds were prepared by combining casting and freeze drying. The preparation process is illustrated in Fig. 1. Briefly, gelatin was added to water and kept at 50 °C under stirring for 3 h to obtain a 3 wt% gelatin solution. Next, different amounts of PSC powders (0.1, 0.5, 1.0 and 5.0 mg/mL) were added to the above gelatin solution under stirring. The resultant mixtures were casted into plastic molds and subsequently frozen at  $-20$  °C overnight. Next, the gelatin/PSC composites were cross-linked with 0.5 wt% glutaraldehyde solution (GA) for 24 h. After crosslinking, the reaction was stopped by 0.1 M glycine, and the obtained composites were washed with water three times. Finally, the G/PSC composite scaffolds were freeze dried for 72 h. The G scaffold was prepared using the same procedure in the absence of PSC.

### 2.3. Characterization of scaffolds

**Appearance of scaffolds:** The surface morphology and structure of the scaffolds were observed by scanning electron microscopy (SEM). Rhodamine B dye (0.01%) was used to label the PSC particles [21], and then Zeiss LSM-710 confocal laser-scanning microscopy (CLSM) was used to observe the distribution of PSC particles.

**Bioactivity test:** The scaffolds (1 mg/mL) were soaked in simulated body fluid (SBF) at 37 °C for 3 days to test the bioactivity. The morphology and crystal type of deposits on the pore wall of the scaffolds were characterized by SEM and X-ray diffraction (XRD). The parameters of XRD measurements were Cu K $\alpha$  radiation ( $\lambda = 1.54 \text{ \AA}$ ), 40 kV and 200 mA, and the data were collected at  $2\theta$  from 15° to 65° by 4°/min.

**Ion concentration and pH:** The scaffolds (1 mg/mL) were soaked in SBF. After 24 h, the concentrations of Si, Ca and P elements in the SBF were detected by inductively coupled plasma mass spectrometry (ICP-MS, iCAP Q, Thermo, USA). The pH value in SBF was monitored regularly using a pH meter (SevenCompact, METTLER TOLEDO, Switzerland).

**Water absorption rate:** All scaffolds ( $d = 8.0$  mm,  $h = 8.0$  mm) were immersed in 20 mL of SBF for 24 h. The weights of the scaffolds before and after SBF soaking were weighed using an analytical balance (ME104T/02; METTLER TOLEDO, Switzerland). The water absorption rate was calculated using the following formula (Eq. (1)).

$$\text{Water absorption rate (\%)} = (w_{\text{after}} - w_{\text{before}}) / w_{\text{before}} \times 100\% \quad (1)$$

**Mechanical test:** Compression tests of the scaffolds ( $d = 8.0$  mm,  $h = 8.0$  mm) after immersion in SBF were performed using an INSTRON 3367 machine (Norwood, MA, USA). The condition of compression was fixed at 100 N, and a crosshead speed of 0.5 mm/min with a maximum compressive strain was set at 30%. The modulus was calculated as the slope of the linear part in the stress-strain curve, and the averages and standard deviations were reported ( $n = 3$ ).

**In vitro degradation evaluation:** The scaffolds (1 mg/mL) were immersed in SBF containing 1 mg/mL of lysozyme at 37 °C. At different time intervals (0, 1, 4, 7 and 10 days), the samples were collected by centrifugation at 5000 rpm and freeze dried for 24 h. The initial mass ( $m_0$ ) and residual mass ( $m_1$ ) were measured, and then the percentages of  $m_1$  to  $m_0$  were used to represent the degradation behavior of the scaffolds (Eq. (2)). The averages and standard deviations were reported ( $n = 3$ ).

$$\text{Residual mass (\%)} = m_1 / m_0 \times 100\% \quad (2)$$

#### 2.4. Cell adhesion, growth and proliferation on scaffolds

Human bone marrow mesenchymal stem cells (hBMMSCs) were obtained from ScienCell Research Laboratories. The cells were cultured in MSCM supplemented with 5% (v/v) FBS, 1% (v/v) MSCGS, 100 U/mL of penicillin and 100 mg/mL of streptomycin. The cells were maintained at 37 °C in 5% CO<sub>2</sub>. hBMMSCs at passages between 3 and 8 were used for experiments.

The scaffolds were sterilized with ethylene oxide and soaked in MSCM at 37 °C overnight before seeding cells. After drying the water from the scaffolds with filter paper, 40  $\mu$ L of the cell suspension ( $1 \times 10^6$  cells/mL) was carefully dripped to the center of the scaffolds, which were then cultured in an incubator at 37 °C for 4 h to allow cell attachment on the scaffolds. The non-adherent cells were eluted by MSCM, and then the scaffolds with hBMMSCs were transferred to new plates for further experiments. The culture medium was changed every 2 days.

**Cell adhesion:** To evaluate hBMMSC adhesion on the scaffolds, scaffolds with hBMMSCs were fixed in 2.5% GA for 30 min after 1 day of culture and dehydrated by gradient ethanol (50%, 75%, 90%, 95% and 100%) and hexamethyl disilylamine (HMDS) for SEM observation.

**Cell growth and proliferation:** At 2 and 7 days of culture, scaffolds with hBMMSCs were fixed in 4% paraformaldehyde for 30 min and stained with 4, 6-diamidino-2-phenylindole (DAPI; Invitrogen, Eugene, OR, USA) for 10 min at room temperature; additionally, the number of cells was observed by CLSM.

The cell proliferation ability in the scaffolds was evaluated using Cell Counting Kit-8 (CCK-8, Dojindo Laboratories, Kyushu Island, Japan) according to the manufacturer's instructions. At 1, 4, 7 and 14 days of culture, the cells seeded on the scaffolds were treated with 10% CCK-8 reagent medium solution and incubated at 37 °C in 5% CO<sub>2</sub> for 2 h. The optical density (OD) value was measured at 450 nm with a reference wavelength of 630 nm. Three individual experiments were performed, and each sample was conducted in triplicate.

**Cell infiltration:** Cell growth in the inside of the scaffolds was observed via histological sections. At 1 and 14 days of culture, the samples were fixed in 2.5% GA for 30 min at room temperature, dehydrated and embedded in paraffin. The sections (5  $\mu$ m) were stained with hematoxylin-eosin (H&E) to observe the growth of cells inside the scaffolds.

**Table 1**

Forward and reverse primers for reverse-transcription polymerase chain reaction.

Gene	Sequences (5'-3')	
<i>DMP-1</i>	Forward:	CTCCGAGTTGGACGATGAGG
	Reverse:	TCATGCTGCACTGTTTCATTC
<i>DSPP</i>	Forward:	ATATTGAGGGCTGGAATGGGGA
	Reverse:	TTTGTGGCTCCAGCATTGTCA
<i>ALP</i>	Forward:	AGCACTCCCACCTTCATCTGGAA
	Reverse:	GAGACCAATAGGTAGTCCACATTG
<i>Col-1</i>	Forward:	CGAAGACATCCCACCAATCAC
	Reverse:	TGTCGAGACGCAGAT
<i>OCN</i>	Forward:	AGGGCAGCGAGGTAGTGA
	Reverse:	CCTGAAAGCCGATGTGGT
<i>Runx2</i>	Forward:	ACCCAGAAGGCACAGACAGAAG
	Reverse:	AGGAATGCGCCCTAAATCACT
<i>18S rRNA</i>	Forward:	GTAAACCCGTTGACCCCAT
	Reverse:	CCATCCAATCGGTAGTAGCG

#### 2.5. Cell migration

The cell migration of hBMMSCs was evaluated by Transwell chambers with an 8  $\mu$ m pore (Becton Dickinson and Company, USA). The scaffolds were soaked in MSCM containing 0.1% FBS at the lower compartment of the chambers. The cells ( $5 \times 10^4$  cells/well) were seeded into the upper compartment. After incubation for 24 h, the membranes of the chambers were fixed with 4% paraformaldehyde for 30 min at room temperature. The cells in the upper chamber were gently wiped with a cotton swab. The cells migrating to the lower side of the membranes were stained with 0.1% crystal violet for 5 min and counted under a microscope in six random nonoverlapping fields. All the experiments were independently repeated three times.

#### 2.6. Odontogenic-related gene expression of hBMMSCs by real-time reverse transcription-polymerase chain reaction (real-time RT-PCR)

The total RNA of each group was extracted using the RNAeasy™ Animal RNA Isolation Kit with Spin Column (Beyotime Bio, China) according to the manufacturer's instructions and then was reverse transcribed into cDNA using the 5  $\times$  PrimeScript RT Master Mix (TaKaRa Bio, Otsu, Japan) at 37 °C for 15 min and 85 °C for 5 s. Real-time RT-PCR was performed using SYBR Green Master Rox (Roche Diagnostics Ltd, Mannheim, Germany) with a 7500 ABI Real-Time PCR System (Applied Biosystems, Foster City, USA). The primer sets used to detect dentin sialophosphoprotein (*DSPP*), dentin matrix protein 1 (*DMP-1*), alkaline phosphatase (*ALP*), collagen type I (*Col-1*), osteocalcin (*OCN*), runt-related transcription factor 2 (*Runx2*) and 18S ribosomal RNA (*18S rRNA*) are shown in Table 1. The relative gene expression was calculated using the  $2^{-\Delta\Delta C_t}$  method, and the *18S rRNA* gene was used as the housekeeping gene. The results were calculated from three independent experiments.

#### 2.7. Statistics

Quantitative results were expressed as the means  $\pm$  standard deviation (SD). One-way analysis of variance (one-way ANOVA) and Bonferroni correction were performed with SPSS 25.0 software, and a *p*-Value less than 0.05 was considered statistically significant.

### 3. Results

#### 3.1. Appearance of scaffolds

The morphology and microstructure of the G/PSC scaffolds are shown in Fig. 2A–I. All the scaffolds were pale yellow discs with a diameter of 8 mm and a thickness of 1 mm (Fig. 2A1–E1). The SEM images of all scaffolds showed an interconnected porous structure with

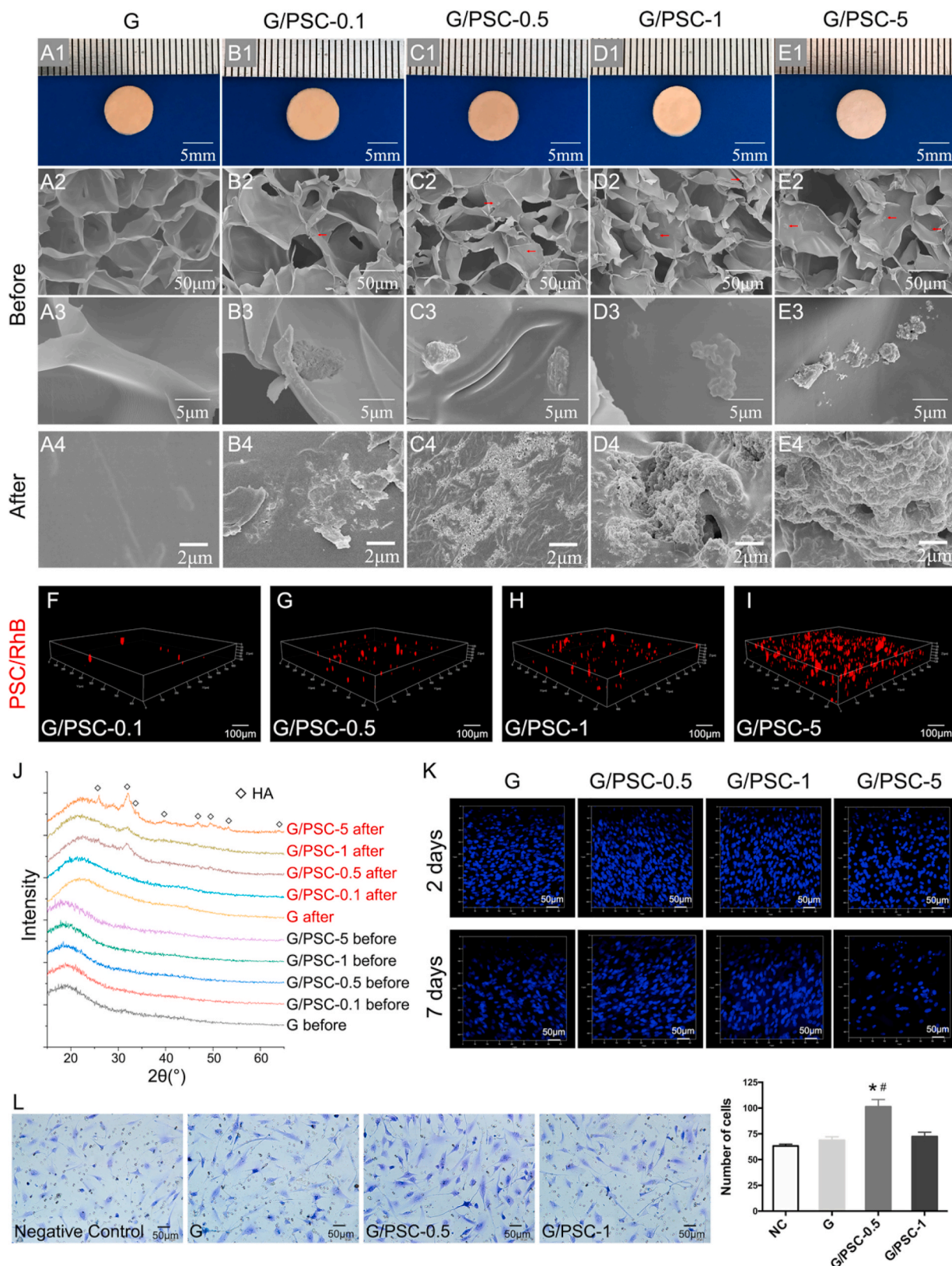


**Fig. 2.** The characteristic and screening of bioactive glass PSC concentration in G/PSC scaffolds. Photographs, SEM micrographs and confocal images of (A1–A4) G scaffold, (B1–B4, F) G/PSC-0.1 scaffold, (C1–C4, G) G/PSC-0.5 scaffold, (D1–D4, H) G/PSC-1 scaffold and (E1–E4, I) G/PSC-5 scaffold before and after immersion in SBF for 3 days. Arrows indicated PSC particles (red). PSC in confocal image sets were stained with Rhodamine B (red). (J) XRD patterns of G and G/PSC scaffolds before and after immersion in SBF for 3 days. (K) Confocal images of hBMMSCs cultured on different scaffolds after 2 and 7 days. Cell nucleus in image sets were stained with DAPI (blue). (L) Transwell cell migration assay (\* $p < 0.05$  vs. NC, # $p < 0.05$  vs. G). HA, hydroxyapatite; NC, negative control.

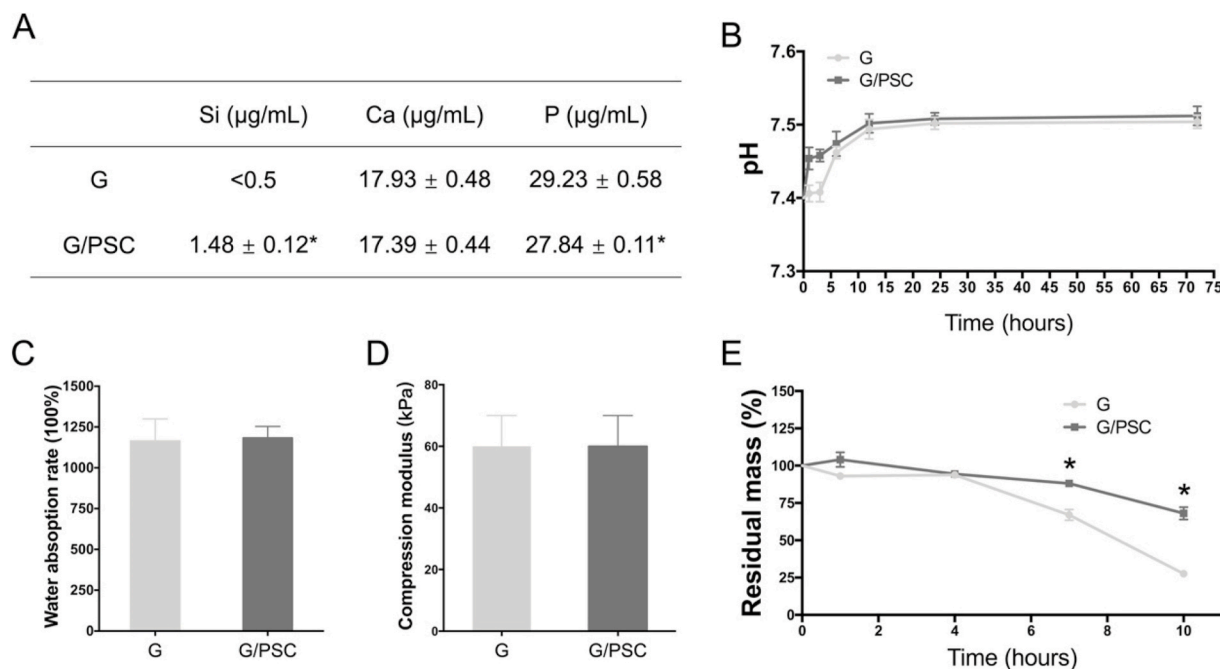


**Fig. 3.** Physicochemical properties of the G and G/PSC scaffolds. (A) Concentration of Si, Ca and P ions in SBF after scaffolds immersion for 24 h ( $*p < 0.05$  vs. G). (B) The pH values of SBF after the scaffolds immersion for 72 h. (C) The water absorption rates and (D) compressive moduli of G and G/PSC scaffolds. (E) Residual masses of G and G/PSC scaffolds with time incubated in SBF containing 1 mg/mL lysozyme ( $*p < 0.05$  vs. G).

pore sizes in the range of 50–150  $\mu\text{m}$  (Fig. 2A2-E2). The pore wall of the G scaffold had a smooth surface, whereas the G/PSC scaffolds exhibited PSC particles of approximately 1–10  $\mu\text{m}$  interspersed on the surface of pore walls (Fig. 2A3-E3). CLSM images showed that the PSC particles with red fluorescence were evenly distributed in the G/PSC scaffolds (Fig. 2F–I).

### 3.2. Effect of the PSC concentration in composite scaffolds on the biological property

**Bioactivity of scaffolds:** The bioactivity of the scaffolds was detected by observing the formation of hydroxyapatite (HA) after immersion in SBF at 37 °C for 3 days. The pore wall of the G scaffold was still smooth (Fig. 2A4). With the increasing PSC content, the mineral deposits on pore walls gradually become denser (Fig. 2B4-E4). The XRD spectra revealed that no HA formed in the G and G/PSC-0.1 scaffolds. However, with increasing PSC content, diffraction peaks of HA (26°, 32°, 34°, 40°, 46°, 49°, 53° and 64°) became more evident (Fig. 2J). The results illustrated that G/PSC scaffolds with PSC contents of 0.5, 1.0, and 5.0 mg/mL possessed solid bioactivity.

**Cell growth on scaffolds:** DAPI staining of the hBMMSC nucleus was used to observe the cell numbers on the scaffolds by CLSM. As shown in Fig. 2K, on both days 2 and 7, the cell numbers on the G/PSC-0.5 scaffold were higher than those of the G scaffold, and the numbers on the G/PSC-1 scaffold were nearly as many as those on the G scaffold. However, the cell numbers on the G/PSC-5 scaffold were less than those on the G scaffold on both days 2 and 7, especially on 7 days. These results indicate that only the G/PSC scaffold with a PSC content of 0.5 mg/mL promotes cell growth.

**Cell chemotaxis of scaffolds:** As shown in Fig. 2L, cells migrated through the polycarbonate membrane under scaffold attraction. Compared with negative control and G scaffold groups, the G/PSC scaffold with a PSC content of 0.5 mg/mL significantly promoted hBMMSC migration ( $p < 0.05$ ), whereas other scaffolds did not exhibit obvious cell chemotaxis.

Overall, considering the results of bioactivity, cell growth and cell migration, the G/PSC scaffold with a PSC content of 0.5 mg per mL of 3%

gelatin solution was selected for further experiments.

### 3.3. Physicochemical properties of scaffolds

**Ion release from scaffolds:** Soluble Si, Ca and P ions released from G and G/PSC scaffold immersion in SBF for 24 h were measured by ICP-MS and the results are shown in Fig. 3A. Compared with the G scaffold, Si ion ( $1.48 \pm 0.12 \mu\text{g/mL}$ ) released from the G/PSC scaffold was significantly higher ( $p < 0.05$ ), the P ion ( $27.84 \pm 0.11 \mu\text{g/mL}$ ) was significantly lower ( $p < 0.05$ ), and the Ca ion ( $17.39 \pm 0.44 \mu\text{g/mL}$ ) showed no significant difference ( $p > 0.05$ ).

**Effect of scaffolds on the pH value:** The pH values of SBF during G and G/PSC scaffold immersion for 72 h are shown in Fig. 3B. At 0–24 h, the pH values of the G and G/PSC scaffolds increased slowly and reached  $7.50 \pm 0.01$  and  $7.51 \pm 0.01$  at 24 h, respectively. At 24–72 h, the pH values of the two groups remained stable and nearly neutral.

**Water absorption rate of scaffolds:** The water absorption rates of the G and G/PSC scaffolds are shown in Fig. 3C. The water absorption rates of the G and G/PSC scaffolds were  $11.6 \pm 1.4$  and  $11.8 \pm 0.7$ , respectively. After soaking in SBF for 24 h, no significant difference was found between the groups ( $p > 0.05$ ).

**Compression modulus of the scaffolds:** The compression moduli of the G and G/PSC scaffolds were examined, as shown in Fig. 3D. The compression moduli of the G and G/PSC scaffolds were  $60 \pm 10$  kPa and  $56 \pm 9$  kPa, respectively, with no significant difference between them ( $p > 0.05$ ).

**In vivo degradation of the scaffolds:** The *in vitro* degradation profiles of the G and G/PSC scaffolds are shown in Fig. 3E. In the early stages (1–4 days), the degradation of the scaffolds was negligible. On the 4th day, the residual masses of the G and G/PSC scaffolds were still  $93.8 \pm 1.4\%$  and  $94.4 \pm 1.3\%$ , respectively, with no significant difference between them ( $p > 0.05$ ). In the later period (4–10 days), the degradation of the G scaffold was dramatically accelerated and that of the G/PSC scaffolds also increased but was much lower than that of the G scaffold. On the 7th day, the residual masses of the G and G/PSC scaffolds were  $65.3 \pm 6.0\%$  and  $88.1 \pm 2.4\%$ , respectively, with a significant difference between them ( $p < 0.05$ ). On the 10th day, the residual mass of the G scaffold was

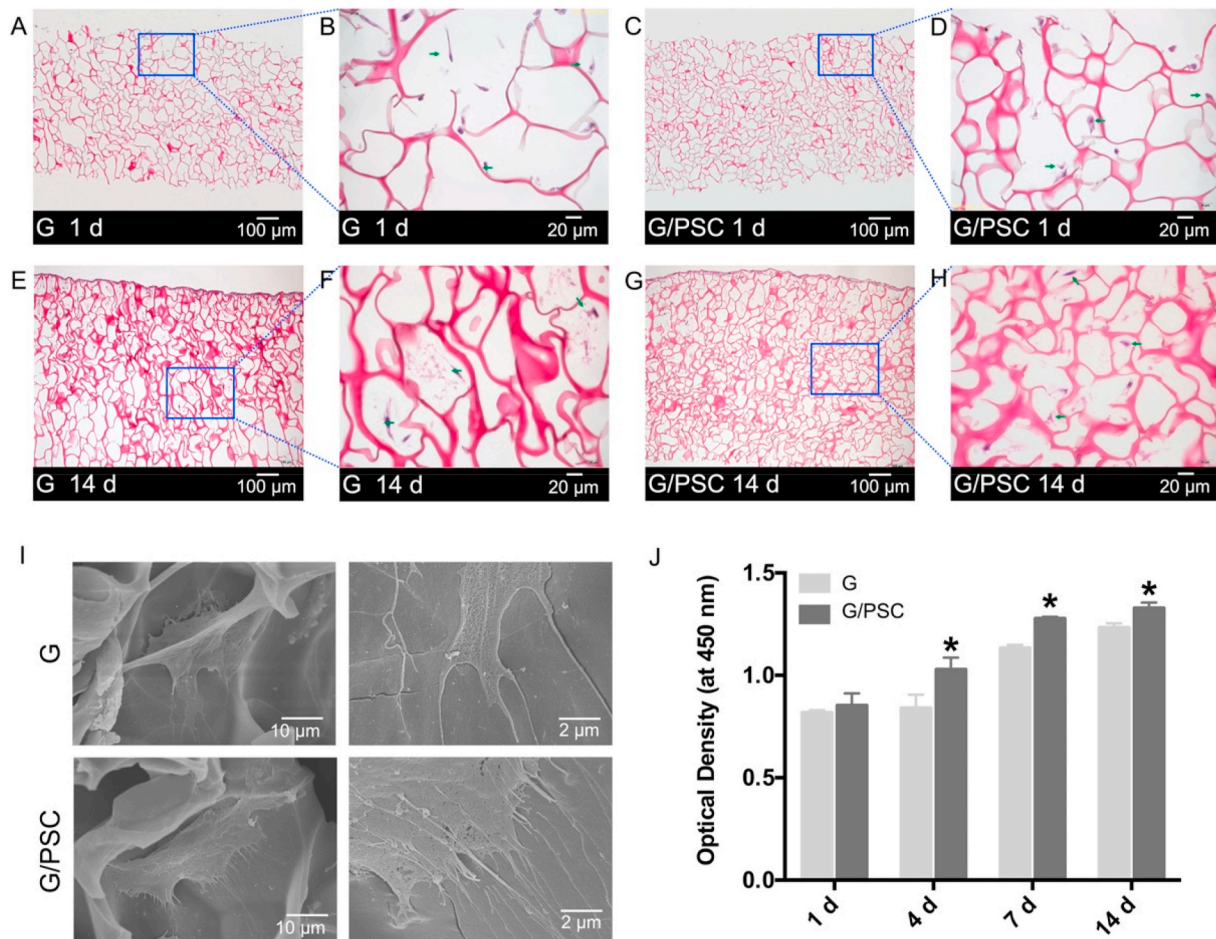


**Fig. 4.** The growth of hBMMSCs on the G and G/PSC scaffolds. H&E staining images of hBMMSCs cultured on (A, E) G and (C, G) G/PSC scaffolds for 1 and 14 days; (B) is the magnification of (A), (D) is the magnification of (C), (F) is the magnification of (E), (H) is the magnification of (G). The (I) cell morphology and (J) proliferation of hBMMSCs on G and G/PSC scaffolds (\* $p < 0.05$  vs. G). H&E, hematoxylin-eosin.

only  $27.6 \pm 1.8\%$  while that of the G/PSC scaffold was still  $68.1 \pm 4.1\%$ , with a significant difference between them ( $p < 0.05$ ).

### 3.4. Growth and proliferation of hBMMSCs on the scaffolds

**Cell adhesion:** As shown in Fig. 4I, hBMMSCs adhered to the pore wall of the G and G/PSC scaffolds. hBMMSCs protruded many pseudopods elongating along the arc of the pore wall or spanning between the pores to closely combine with the matrix of scaffolds with a fusiform or polygon spreading shape. Notably, the number of pseudopods of hBMMSCs on the G/PSC scaffold was greater than that on the G scaffold.

**Cell infiltration:** H&E staining was performed to further characterize the growth of the infiltrated hBMMSCs inside the scaffolds. As shown in Fig. 4A–D, no obvious cell infiltration was observed after 1 day. When cultured *in vitro* for 14 days, hBMMSCs had infiltrated into the inner region of the G and G/PSC scaffolds along the interconnected pores and reached a depth approximately 600 μm in both scaffolds (Fig. 4E–H). The whole or part of the cell structure, including blue-stained nuclear and pink-stained cytoplasm, could be seen in these two scaffolds (Fig. 4F, H).

**Cell proliferation:** The CCK-8 assay was performed to observe the number of hBMMSCs on the G and G/PSC scaffolds. During the 14 days of cell culture, hBMMSCs continued to proliferate on the G and G/PSC scaffolds (Fig. 4J). The number of cells on the G/PSC scaffold was significantly higher than that of the G scaffold from 4 to 14 days ( $p < 0.05$ ), indicating that the G/PSC scaffold could promote hBMMSC proliferation compared with the G scaffold.

### 3.5. Stimulation of the odontogenic differentiation of hBMMSCs by the scaffolds

Real-time RT-PCR was carried out to analyze odontogenic-related gene expression of hBMMSCs cultured on the G and G/PSC scaffolds after 4 and 14 days. The mRNA expression levels of *DSPP*, *OCN*, *ALP*, *Runx2*, and *Col-1* were significantly up-regulated by the G/PSC scaffold compared with those on the G scaffold after both 4 and 14 days (Fig. 5A, C–F). *DMP-1* expression was also upregulated by the G/PSC scaffold, but not the G scaffold, after 14 days of culture (Fig. 5B). Additionally, the expression levels of both *DSPP* and *DMP-1* in hBMMSCs on the G/PSC scaffold increased by more than 6-fold compared with that on the G scaffold group after 14 days. These results demonstrate that the G/PSC scaffold could induce hBMMSCs to undergo odontogenic differentiation.

## 4. Discussion

Both dentin and bone are highly mineralized tissues with similar chemical compositions and formation mechanisms. Many genes related to mineralization are highly expressed during the odonto/osteogenic differentiation of MSCs, such as *ALP*, *Col-1*, *OCN* and *Runx2* [22–26]. *DSPP* and *DMP-1* are abundantly expressed in dentin but is hardly expressed in bone and are generally considered as the specific markers for odontogenic differentiation [27,28]. The results of this study showed that the migration, proliferation and expression of the odontogenic-specific marker genes *DSPP* and *DMP-1* of hBMMSCs on the G/PSC scaffold were significantly promoted, indicating that hBMMSCs

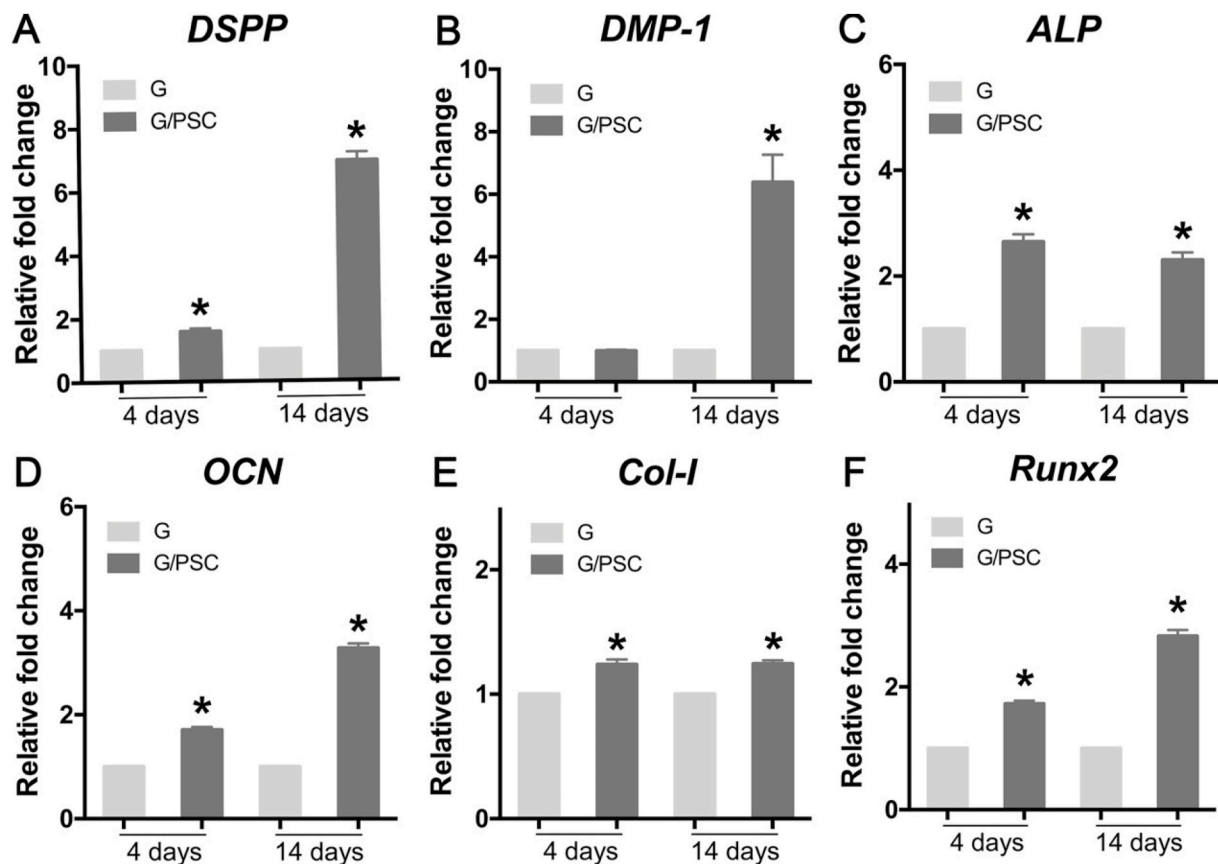


Fig. 5. Odontogenic-related genes expression in hBMMSCs cultured on the G and G/PSC scaffolds for 4 and 14 days (\* $p < 0.05$  vs. G). *DSPP*, dentin sialophosphoprotein; *DMP-1*, dentin matrix protein 1; *ALP*, alkaline phosphatase; *OCN*, osteocalcin; *Runx2*, runt-related transcription factor 2; *Col-1*, collagen type I.

had undergone odontogenic differentiation on the newly prepared scaffolds. MSCs can differentiate into diverse lineages, and their differentiations are highly dependent on their microenvironments in situ [29]. The scaffolds not only support cellular adhesion and growth but also provide the microenvironment for the differentiation of MSCs [30]. Cells could respond to the physicochemical stimulations of the scaffolds by adjusting their behaviors, including cell adhesion, migration, proliferation and differentiation.

PSC is an important component of the G/PSC scaffold, which could provide the microenvironment to induce hBMMSCs to undergo odontogenic differentiation. Our previous studies demonstrated that BG promotes the proliferation, differentiation and mineralization of hDPCs and could also induces dental pulp tissue to form a dentin-pulp complex-like structure *in vivo* [14,15,20]. Kim et al. [31] also revealed that the addition of BG into polycaprolactone-gelatin scaffolds could upregulate the expression of the genes *DSPP*, *DMP-1*, *ALP*, *OCN* and *Runx2* of hDPCs. Previous studies have found that the effects of BG on cells are dose-dependent and might be related to the concentrations of soluble Si, Ca and P ions. If the BG content is too low, exhibiting bioactivity through HA formation is difficult [32]. However, excessive BG leads to cell cytotoxicity due to the ion burst release [15,33]. Xing et al. [34] concluded that Si ion at 1.30–5.18  $\mu\text{g}/\text{mL}$  in the medium significantly promoted BMMSC proliferation; however, the proliferation was inhibited at a higher concentration of Si ion. BG-coated dentin slices at 0.5 mg/mL showed a significant enhancement effect on the early adhesion and migration of BMMSCs [17]. In the present study, the Si ion concentration released from the G/PSC scaffold was  $1.48 \pm 0.12 \mu\text{g}/\text{mL}$ , and the results confirmed that it significantly promoted hBMMSC proliferation and migration. Additionally, on the G/PSC scaffold, hBMMSCs had more protruding pseudopodia, consistent with previous findings [35, 36]. It should be noted that this study only tested the effects of the PSC

content on cell proliferation and migration of hBMMSCs but not cell differentiation.

The physical properties of the scaffold, such as pore size and stiffness, play important roles in regulating cellular behaviors. Concerning pore size, Jiang et al. [37] investigated the mechano-responsiveness of fibroblasts to scaffolds with different pore sizes (30  $\mu\text{m}$  and 80  $\mu\text{m}$ ). They found that fibroblasts were sensitive to pore size, and the 80  $\mu\text{m}$  pore was more helpful to cell adhesion and migration on the scaffold. Lee et al. [38] prepared multiphase scaffolds with different pore sizes using 3D printing technology, and the results revealed that the 100  $\mu\text{m}$  pore induced DPSCs to differentiate into odontoblasts, while DPSCs on the 300  $\mu\text{m}$  pore area were prone to differentiate into the osteogenic lineage. Regarding the mechanical property, Qu et al. [39] explored the effects of stiffness (0.23–24.25 kPa) of gelatin scaffolds on the biological behaviors of DPSCs. Their experiments showed that the scaffold with a compression modulus of 24.25 kPa was favored for the odontogenic differentiation of DPSCs. Another study demonstrated that a stiffer polydimethylsiloxane matrix membrane (54–135 kPa) could accelerate the odontogenic differentiation of DPSCs [40]. The pore size and mechanical property could be regulated by controlling the composition and preparation conditions [41–43]. To facilitate the odontogenic differentiation of MSCs, the pore size and stiffness of the scaffolds are subtly designed. In this study, the concentration of gelatin was 3 wt% in the starting solution, the freezing temperature was  $-20^\circ\text{C}$ . GA is widely used as a crosslinking agent, and the change of GA's concentration could be used to modulate the physicochemical properties of biomaterials. It was reported that gelatin crosslinked with 0.5% (w/v) GA had a moderate crosslinking degree and mechanical properties, at the meanwhile no obvious cytotoxicity was detected [44–46]. Therefore, in this study, we adopted the concentration of 0.5% (w/v) GA as the crosslinking agent. In order to further improve the biocompatibility of the gelatin

scaffolds crosslinked by GA, a glycine solution containing free amine groups was used to wash the scaffolds [47]. The results have shown that G and G/PSC scaffolds prepared in present study had few cytotoxicity, with a pore size of approximately 100  $\mu\text{m}$  and a compression modulus of 50–60 kPa, which created a conducive microenvironment for odontogenic differentiation. The results displayed that *DMP-1* expression in hBMMSCs was not only significantly increased on the G/PSC scaffold but could also be detected on the G scaffold. Previous studies confirmed that BMMSCs cannot express the odontogenic-specific gene *DMP-1* without induction [7,48]. Thus, the current results preliminarily indicated that the G/PSC scaffold prepared by the combination of PSC BG and appropriate physical properties possessed the abilities of chemotaxis and odontogenic differentiation of BMMSCs. Pulp regeneration will be affected by the growth factors released from dentin [49,50], which may further promote the odontogenic differentiation of BMMSCs on the scaffold used in situ.

## 5. Conclusions

The G/PSC scaffold prepared by PSC content of 0.5 mg/mL in 3% gelatin solution has shown good mineralization activity, cell biocompatibility, and possessed well-defined pores ( $\sim 100 \mu\text{m}$ ) and befitting stiffness (50–60 kPa) for pulp regeneration. Through releasing ions and HA formation, PSC endowed the scaffold with bioactivity, which significantly promoted the chemotaxis, adhesion, proliferation and odontogenic differentiation of hBMMSCs. The present results suggest that the G/PSC scaffold could provide an appropriate odontogenic microenvironment. Therefore, whether the G/PSC scaffold has potential for pulp regeneration is worthy of further investigation.

## Author contribution statement

**Guibin Huang:** Methodology, Investigation, Formal analysis, Writing-original draft. **Liju Xu:** Data curation. **Jilin Wu:** Data curation. **Sainan Wang:** Assistance of Project administration, Writing-Review & Editing, Co-Supervision, Funding acquisition. **Yanmei Dong:** Conceptualization, Funding acquisition, Supervision, Project administration, Writing - Review & Editing.

## Declaration of competing interest

The authors declare that they have no known competing financial interests or personal relationships that could have appeared to influence the work reported in this paper.

## Acknowledgements

Authors are grateful to Wooquick (Taizhou, China) for kindly providing the pH-neutral bioactive glass PSC. This work was supported by the National Natural Science Foundation of China (grant numbers 81870753, 81700953).

## Appendix A. Supplementary data

Supplementary data to this article can be found online at <https://doi.org/10.1016/j.polymertesting.2020.106915>.

## References

- [1] S. Eramo, A. Natali, R. Pinna, E. Milia, Dental pulp regeneration via cell homing, *Int. Endod. J.* (2017), <https://doi.org/10.1111/iej.12868>.
- [2] T.W. Lovelace, M.A. Henry, K.M. Hargreaves, A. Diogenes, Evaluation of the delivery of mesenchymal stem cells into the root canal space of necrotic immature teeth after clinical regenerative endodontic procedure, *J. Endod.* 37 (2) (2011) 133–138, <https://doi.org/10.1016/j.joen.2010.10.009>.
- [3] Y. Yamada, A. Fujimoto, A. Ito, R. Yoshimi, M. Ueda, Cluster analysis and gene expression profiles: a cDNA microarray system-based comparison between human dental pulp stem cells (hDPSCs) and human mesenchymal stem cells (hMSCs) for tissue engineering cell therapy, *Biomaterials* 27 (20) (2006) 3766–3781, <https://doi.org/10.1016/j.biomaterials.2006.02.009>.
- [4] M. Altai, L. Richards, G. Rossi-Fedeles, Histological assessment of regenerative endodontic treatment in animal studies with different scaffolds: a systematic review, *Dent. Traumatol.* 33 (4) (2017) 235–244, <https://doi.org/10.1111/edt.12338>.
- [5] M. Frozoni, M.R. Marques, S.K. Hamasaki, N.T. Mohara, A. de Jesus Soares, A. A. Zaia, Contribution of bone marrow-derived cells to reparative dentinogenesis using bone marrow transplantation model, *J. Endod.* 46 (3) (2020) 404–412, <https://doi.org/10.1016/j.joen.2019.12.003>.
- [6] A. Ohazama, S.A.C. Modino, I. Miletich, P.T. Sharpe, Stem-cell-based tissue engineering of murine teeth, *J. Dent. Res.* 83 (7) (2004) 518–522, <https://doi.org/10.1177/154405910408300702>.
- [7] Z.Y. Li, L. Chen, L. Liu, Y.F. Lin, S.W. Li, W.D. Tian, Odontogenic potential of bone marrow mesenchymal stem cells, *J. Oral Maxillofac. Surg.* 65 (3) (2007) 494–500, <https://doi.org/10.1016/j.joms.2006.09.018>.
- [8] J.M. Zheng, Y.Y. Kong, Y.Y. Li, W. Zhang, MagT1 regulated the odontogenic differentiation of BMMSCs induced by TGC-CM via ERK signaling pathway, *Stem Cell Res. Ther.* 10 (1) (2019) 48, <https://doi.org/10.1186/s13287-019-1148-6>.
- [9] G. Lei, Y. Yu, Y. Jiang, S. Wang, M. Yan, A.J. Smith, G. Smith, P.R. Cooper, C. Tang, G. Zhang, J. Yu, Differentiation of BMMSCs into odontoblast-like cells induced by natural dentine matrix, *Arch. Oral Biol.* 58 (7) (2013) 862–870, <https://doi.org/10.1016/j.archoralbio.2013.01.002>.
- [10] B. Hashmi, T. Mammoto, J. Weaver, T. Ferrante, A. Jiang, E. Jiang, J. Feliz, D. E. Ingber, Mechanical induction of dentin-like differentiation by adult mouse bone marrow stromal cells using compressive scaffolds, *Stem Cell Res.* 24 (2017) 55–60, <https://doi.org/10.1016/j.scr.2017.08.011>.
- [11] N.R. Kim, D.H. Lee, P.H. Chung, H.C. Yang, Distinct differentiation properties of human dental pulp cells on collagen, gelatin, and chitosan scaffolds, *Oral Surg. Oral Med. Oral Pathol. Oral Radiol. Endod.* 108 (5) (2009) e94–100, <https://doi.org/10.1016/j.tripleo.2009.07.031>.
- [12] L. Londero Cde, C.M. Pagliarin, M.C. Felipe, W.T. Felipe, C.C. Danesi, F. B. Barletta, Histologic analysis of the influence of a gelatin-based scaffold in the repair of immature dog teeth subjected to regenerative endodontic treatment, *J. Endod.* 41 (10) (2015) 1619–1625, <https://doi.org/10.1016/j.joen.2015.01.033>.
- [13] H. Ishimatsu, C. Kitamura, T. Morotomi, Y. Tabata, T. Nishihara, K.K. Chen, M. Terashita, Formation of dentinal bridge on surface of regenerated dental pulp in dentin defects by controlled release of fibroblast growth factor-2 from gelatin hydrogels, *J. Endod.* 35 (6) (2009) 858–865, <https://doi.org/10.1016/j.joen.2009.03.049>.
- [14] W. Gong, Z. Huang, Y. Dong, Y. Gan, S. Li, X. Gao, X. Chen, Ionic extraction of a novel nano-sized bioactive glass enhances differentiation and mineralization of human dental pulp cells, *J. Endod.* 40 (1) (2014) 83–88, <https://doi.org/10.1016/j.joen.2013.08.018>.
- [15] S. Wang, X. Gao, W. Gong, Z. Zhang, X. Chen, Y. Dong, Odontogenic differentiation and dentin formation of dental pulp cells under nanobioactive glass induction, *Acta Biomater.* 10 (6) (2014) 2792–2803, <https://doi.org/10.1016/j.actbio.2014.02.013>.
- [16] S. Wang, Q. Hu, X. Gao, Y. Dong, Characteristics and effects on dental pulp cells of a polycaprolactone/submicron bioactive glass composite scaffold, *J. Endod.* 42 (7) (2016) 1070–1075, <https://doi.org/10.1016/j.joen.2016.04.023>.
- [17] S. Wang, G. Huang, Y. Dong, Directional migration and odontogenic differentiation of bone marrow stem cells induced by dentin coated with nanobioactive glass, *J. Endod.* 46 (2) (2020) 216–223, <https://doi.org/10.1016/j.joen.2019.11.004>.
- [18] A.L. Li, Y. Lv, H.H. Ren, Y. Cui, C. Wang, R.A. Martin, D. Qiu, In vitro evaluation of a novel pH neutral calcium phosphosilicate bioactive glass that does not require preconditioning prior to use, *Int. J. Appl. Glass Sci.* 8 (4) (2017) 403–411, <https://doi.org/10.1111/ijag.12321>.
- [19] A. Li, D. Qiu, Phytic acid derived bioactive CaO-P2O5-SiO2 gel-glasses, *J. Mater. Sci. Mater. Med.* 22 (12) (2011) 2685–2691, <https://doi.org/10.1007/s10856-011-4464-7>.
- [20] C.Y. Cui, S.N. Wang, H.H. Ren, A.L. Li, D. Qiu, Y.H. Gan, Y.M. Dong, Regeneration of dental-pulp complex-like tissue using phytic acid derived bioactive glasses, *RSC Adv.* 7 (36) (2017) 22063–22070, <https://doi.org/10.1039/c7ra01480e>.
- [21] L. Xu, S. Gao, R. Zhou, F. Zhou, Y. Qiao, D. Qiu, Bioactive pore-forming bone adhesives facilitating cell ingrowth for fracture healing, *Adv. Mater.* (2020), e1907491, <https://doi.org/10.1002/adma.201907491>.
- [22] M. Nakashima, Establishment of primary cultures of pulp cells from bovine permanent incisors, *Arch. Oral Biol.* 36 (9) (1991) 655–663, [https://doi.org/10.1016/0003-9969\(91\)90018-p](https://doi.org/10.1016/0003-9969(91)90018-p).
- [23] W.T. Su, P.S. Wu, C.S. Ko, T.Y. Huang, Osteogenic differentiation and mineralization of human exfoliated deciduous teeth stem cells on modified chitosan scaffold, *Mater. Sci. Eng. C Mater. Biol. Appl.* 41 (2014) 152–160, <https://doi.org/10.1016/j.msec.2014.04.048>.
- [24] U. Stucki, J. Schmid, C.F. Hammerle, N.P. Lang, Temporal and local appearance of alkaline phosphatase activity in early stages of guided bone regeneration. A descriptive histochemical study in humans, *Clin. Oral Implants Res.* 12 (2) (2001) 121–127, <https://doi.org/10.1034/j.1600-0501.2001.012002121.x>.
- [25] H. Sun, C. Wu, K. Dai, J. Chang, T. Tang, Proliferation and osteoblastic differentiation of human bone marrow-derived stromal cells on akermanite-bioactive ceramics, *Biomaterials* 27 (33) (2006) 5651–5657, <https://doi.org/10.1016/j.biomaterials.2006.07.027>.
- [26] A. Bakopoulou, G. Leyhausen, J. Volk, A. Tsiptsoglou, P. Garefis, P. Koidis, W. Geurtsen, Comparative analysis of in vitro osteo/odontogenic differentiation potential of human dental pulp stem cells (DPSCs) and stem cells from the apical

- papilla (SCAP), *Arch. Oral Biol.* 56 (7) (2011) 709–721, <https://doi.org/10.1016/j.archoralbio.2010.12.008>.
- [27] S. Chen, J. Gluhak-Heinrich, Y.H. Wang, Y.M. Wu, H.H. Chuang, L. Chen, G. H. Yuan, J. Dong, I. Gay, M. MacDougall, Runx2, osx, and dspp in tooth development, *J. Dent. Res.* 88 (10) (2009) 904–909, <https://doi.org/10.1177/0022034509342873>.
- [28] R.N. D'Souza, A. Cavender, G. Sunavala, J. Alvarez, T. Ohshima, A.B. Kulkarni, M. MacDougall, Gene expression patterns of murine dentin matrix protein 1 (Dmp1) and dentin sialophosphoprotein (DSPP) suggest distinct developmental functions in vivo, *J. Bone Miner. Res.* 12 (12) (1997) 2040–2049, <https://doi.org/10.1359/jbmr.1997.12.12.2040>.
- [29] A.S. Vidane, H.D. Zomer, B.M. Oliveira, C.F. Guimaraes, C.B. Fernandes, F. Percin, L.A. Silva, M.A. Miglino, F.V. Meirelles, C.E. Ambrosio, Reproductive stem cell differentiation: extracellular matrix, tissue microenvironment, and growth factors direct the mesenchymal stem cell lineage commitment, *Reprod. Sci.* 20 (10) (2013) 1137–1143, <https://doi.org/10.1177/1933719113477484>.
- [30] K.M. Galler, R.N. D'Souza, J.D. Hartgerink, G. Schmalz, Scaffolds for dental pulp tissue engineering, *Adv. Dent. Res.* 23 (3) (2011) 333–339, <https://doi.org/10.1177/0022034511405326>.
- [31] G.H. Kim, Y.D. Park, S.Y. Lee, A. El-Fiqi, J.J. Kim, E.J. Lee, H.W. Kim, E.C. Kim, Odontogenic stimulation of human dental pulp cells with bioactive nanocomposite fiber, *J. Biomater. Appl.* 29 (6) (2015) 854–866, <https://doi.org/10.1177/0885328214546884>.
- [32] C. Ohtsuki, T. Kokubo, T. Yamamuro, Mechanism of apatite formation on CaO-SiO<sub>2</sub>-P<sub>2</sub>O<sub>5</sub> glasses in a simulated body-fluid, *J. Non-Cryst. Solids* 143 (1) (1992) 84–92, [https://doi.org/10.1016/S0022-3093\(05\)80556-3](https://doi.org/10.1016/S0022-3093(05)80556-3).
- [33] A. Hoppe, N.S. Guldal, A.R. Boccaccini, A review of the biological response to ionic dissolution products from bioactive glasses and glass-ceramics, *Biomaterials* 32 (11) (2011) 2757–2774, <https://doi.org/10.1016/j.biomaterials.2011.01.004>.
- [34] M. Xing, X. Wang, E. Wang, L. Gao, J. Chang, Bone tissue engineering strategy based on the synergistic effects of silicon and strontium ions, *Acta Biomater.* 72 (2018) 381–395, <https://doi.org/10.1016/j.actbio.2018.03.051>.
- [35] T. Chae, H. Yang, V. Leung, F. Ko, T. Troczynski, Novel biomimetic hydroxyapatite/alginate nanocomposite fibrous scaffolds for bone tissue regeneration, *J. Mater. Sci. Mater. Med.* 24 (8) (2013) 1885–1894, <https://doi.org/10.1007/s10856-013-4957-7>.
- [36] S. Fanaee, S. Labbaf, M.H. Enayati, A. Baharlou Houreh, M.N. Esfahani, Creation of a unique architectural structure of bioactive glass sub-micron particles incorporated in a polycaprolactone/gelatin fibrous mat; characterization, bioactivity, and cellular evaluations, *J. Biomed. Mater. Res.* 107 (7) (2019) 1358–1365, <https://doi.org/10.1002/jbm.a.36649>.
- [37] S. Jiang, C. Lyu, P. Zhao, W. Li, W. Kong, C. Huang, G.M. Genin, Y. Du, Cryoprotectant enables structural control of porous scaffolds for exploration of cellular mechano-responsiveness in 3D, *Nat. Commun.* 10 (1) (2019) 3491, <https://doi.org/10.1038/s41467-019-11397-1>.
- [38] C.H. Lee, J. Hajibandeh, T. Suzuki, A. Fan, P. Shang, J.J. Mao, Three-dimensional printed multiphase scaffolds for regeneration of periodontium complex, *Tissue Eng. A* 20 (7–8) (2014) 1342–1351, <https://doi.org/10.1089/ten.TEA.2013.0386>.
- [39] T. Qu, J. Jing, Y. Ren, C. Ma, J.Q. Feng, Q. Yu, X. Liu, Complete pulpodentinal complex regeneration by modulating the stiffness of biomimetic matrix, *Acta Biomater.* 16 (2015) 60–70, <https://doi.org/10.1016/j.actbio.2015.01.029>.
- [40] N. Liu, M. Zhou, Q. Zhang, T. Zhang, T. Tian, Q. Ma, C. Xue, S. Lin, X. Cai, Stiffness regulates the proliferation and osteogenic/odontogenic differentiation of human dental pulp stem cells via the WNT signalling pathway, *Cell Prolif* 51 (2) (2018), e12435, <https://doi.org/10.1111/cpr.12435>.
- [41] N. Arabi, A. Zamanian, Effect of cooling rate and gelatin concentration on the microstructural and mechanical properties of ice template gelatin scaffolds, *Biotechnol. Appl. Biochem.* 60 (6) (2013) 573–579, <https://doi.org/10.1002/bab.1120>.
- [42] Y. Yang, A.C. Ritchie, N.M. Everitt, Comparison of glutaraldehyde and procyanidin cross-linked scaffolds for soft tissue engineering, *Mater. Sci. Eng. C Mater. Biol. Appl.* 80 (2017) 263–273, <https://doi.org/10.1016/j.msec.2017.05.141>.
- [43] A. Oryan, A. Kamali, A. Moshiri, H. Baharvand, H. Daemi, Chemical crosslinking of biopolymeric scaffolds: current knowledge and future directions of crosslinked engineered bone scaffolds, *Int. J. Biol. Macromol.* 107 (Pt A) (2018) 678–688, <https://doi.org/10.1016/j.ijbiomac.2017.08.184>.
- [44] A. Bigi, G. Cojazzi, S. Panzavolta, K. Rubini, N. Roveri, Mechanical and thermal properties of gelatin films at different degrees of glutaraldehyde crosslinking, *Biomaterials* 22 (8) (2001) 763–768, [https://doi.org/10.1016/S0142-9612\(00\)00236-2](https://doi.org/10.1016/S0142-9612(00)00236-2).
- [45] Mahmoud Azami, Mohammad Rabiee, F. Moztaaradeh, Glutaraldehyde crosslinked gelatin/hydroxyapatite nanocomposite scaffold, engineered via compound techniques, *Polym. Compos.* 31 (2010) 2112–2120, <https://doi.org/10.1002/pc.21008>.
- [46] R. Imani, M. Rafienia, S.H. Emami, Synthesis and characterization of glutaraldehyde-based crosslinked gelatin as a local hemostat sponge in surgery: an in vitro study, *Bio Med. Mater. Eng.* 23 (3) (2013) 211–224, <https://doi.org/10.3233/BME-130745>.
- [47] N.W. Guldner, I. Jasmund, H. Zimmermann, M. Heinlein, B. Girndt, V. Meier, F. Fluss, D. Rohde, A. Gebert, H.H. Sievers, Detoxification and endothelialization of glutaraldehyde-fixed bovine pericardium with titanium coating A new technology for cardiovascular tissue engineering, *Circulation* 119 (12) (2009) 1653–1660, <https://doi.org/10.1161/Circulationaha.108.823948>.
- [48] F. Mashhadi Abbas, H. Sichani Fallahi, A. Khoshzaban, N. Mahdavi, S.S. Bagheri, Expression of odontogenic genes in human bone marrow mesenchymal stem cells, *Cell J* 15 (2) (2013) 136–141, <https://doi.org/10.1111/boc.201390011>.
- [49] K.M. Galler, M. Widbiller, W. Buchalla, A. Eidt, K.A. Hiller, P.C. Hoffer, G. Schmalz, EDTA conditioning of dentine promotes adhesion, migration and differentiation of dental pulp stem cells, *Int. Endod. J.* 49 (6) (2016) 581–590, <https://doi.org/10.1111/iej.12492>.
- [50] K.M. Galler, W. Buchalla, K.A. Hiller, M. Federlin, A. Eidt, M. Schiefersteiner, G. Schmalz, Influence of root canal disinfectants on growth factor release from dentin, *J. Endod.* 41 (3) (2015) 363–368, <https://doi.org/10.1016/j.joen.2014.11.021>.